Quantification of Compartmented Metabolic Fluxes in Developing Soybean Embryos by Employing Biosynthetically Directed Fractional ^{13}C Labeling, Two-Dimensional [^{13}C, ^{1}H] Nuclear Magnetic Resonance, and Comprehensive Isotopomer Balancing[1][w]

Ganesh Sriram, D. Bruce Fulton, Vidya V. Iyer, Joan Marie Peterson, Ruilian Zhou, Mark E. Westgate, Martin H. Spalding, and Jacqueline V. Shanks*

Departments of Chemical Engineering (G.S., V.V.I., J.V.S.), Biochemistry, Biophysics and Molecular Biology (D.B.F.), Agronomy (J.M.P., R.Z., M.E.W.), and Genetics, Development and Cell Biology (M.H.S.), Iowa State University, Ames, Iowa 50011

Metabolic flux quantification in plants is instrumental in the detailed understanding of metabolism but is difficult to perform on a systemic level. Toward this aim, we report the development and application of a computer-aided metabolic flux analysis tool that enables the concurrent evaluation of fluxes in several primary metabolic pathways. Labeling experiments were performed by feeding a mixture of U-^{13}C Suc, naturally abundant Suc, and Gln to developing soybean (*Glycine max*) embryos. Two-dimensional [^{13}C, ^{1}H] NMR spectra of seed storage protein and starch hydrolysates were acquired and yielded a labeling data set consisting of 155 ^{13}C isotopomer abundances. We developed a computer program to automatically calculate fluxes from this data. This program accepts a user-defined metabolic network model and incorporates recent mathematical advances toward accurate and efficient flux evaluation. Fluxes were calculated and statistical analysis was performed to obtain SDs. A high flux was found through the oxidative pentose phosphate pathway (19.99 ± 4.39 μmol d^{-1} cotyledon^{-1}, or 104.2 carbon mol ± 23.0 carbon mol per 100 carbon mol of Suc uptake). Separate transketolase and transaldolase fluxes could be distinguished in the plastid and the cytosol, and those in the plastid were found to be at least 6-fold higher. The backflux from triose to hexose phosphate was also found to be substantial in the plastid (21.72 ± 5.00 μmol d^{-1} cotyledon^{-1}, or 113.2 carbon mol ±26.0 carbon mol per 100 carbon mol of Suc uptake). Forward and backward directions of anaplerotic fluxes could be distinguished. The glyoxylate shunt flux was found to be negligible. Such a generic flux analysis tool can serve as a quantitative tool for metabolic studies and phenotype comparisons and can be extended to other plant systems.

The evaluation of metabolic flux is instrumental in understanding carbon partitioning in plant metabolism. Since fluxes provide a quantitative depiction of carbon flow through competing metabolic pathways (Ratcliffe and Shachar-Hill, 2001), they are an important physiological characteristic akin to levels of transcripts, proteins, and metabolites (Sauer, 2004). Flux measurements and comparisons of fluxes between phenotypes can provide insights toward selection of appropriate metabolic engineering targets (Stephanopoulos, 1999, 2002; Glawischnig et al., 2002) and toward the construction of predictive models of plant metabolism (Ratcliffe and Shachar-Hill, 2001), the necessity for which has been emphasized recently (Girke et al., 2003; Katagiri, 2003; Raikhel and Coruzzi, 2003).

Although the importance of flux measurement in plants has often been stressed (Roscher et al., 2000; Ratcliffe and Shachar-Hill, 2001; Shachar-Hill, 2002; Sweetlove et al., 2003), it has received rather limited attention in plant science as compared to profiling technologies for transcript, protein, and metabolite levels (Kruger and von Schaewen, 2003; Sweetlove et al., 2003). This is principally due to the fact that fluxes have to be quantified by back-calculating them from their effect on the distribution of a labeled substrate, and such calculation requires a detailed mathematical model if it is to be accurate. Mathematical models relating labeling data to fluxes are often nontrivial, particularly in the case of compartmented metabolism inherent in plants. Consequently, flux measurement technology in plants remains underdeveloped (Ratcliffe and Shachar-Hill, 2001; Sweetlove et al., 2003).

[1] This work was supported by the Division of Bioengineering and Environmental Systems (BES) of the National Science Foundation (grant no. BES–0224600), by the Plant Sciences Institute of Iowa State University, and by the Iowa Soybean Promotion Board.

* Corresponding author; e-mail jshanks@iastate.edu; fax 515–294–2689.

[w] The online version of this article contains Web-only data.

Article, publication date, and citation information can be found at www.plantphysiol.org/cgi/doi/10.1104/pp.104.050625.

Not surprisingly, most papers that have reported labeling studies in plants have focused on the qualitative goal of inferring which pathways are in operation (identification of metabolic network topology) but not on the mathematically involved endeavor of evaluating how much carbon is processed by those pathways (quantification of flux). For example, Wheeler et al. (1998) delineated the pathway of ascorbic acid synthesis in higher plants from ^{14}C labeling data, and Krook et al. (1998) showed that two separate oxidative pentose phosphate pathways (oxPPP) operate in the cytosol and the plastid, using ^{13}C enrichment data from *Daucus carota* cell suspensions. More recently, a suite of articles by Eisenreich and co-workers (Bacher et al., 1999; Glawischnig et al., 2000, 2001, 2002) reported the abundances of isotopomers of several isolated sink metabolites in maize (*Zea mays*) kernels. Although these articles demonstrated advances in label measurement technology, the inferences from them were either qualitative or semiquantitative.

Two recent pioneering research efforts have concentrated on quantification of fluxes in plants. In the first, Raymond and co-workers calculated fluxes through glycolysis, oxPPP, tricarboxylic acid (TCA) cycle, and anaplerotic reactions using ^{13}C atom enrichment data of metabolites isolated from tomato (*Lycopersicon esculentum*) suspension cells (Rontein et al., 2002) and maize root tips (Dieuaide-Noubhani et al., 1995). However, ^{13}C isotopomer abundance data provide richer metabolic information than ^{13}C atom enrichments. Isotopomers are isomers of a metabolite that differ in the labeling state (^{13}C or ^{12}C) of their individual carbon atoms (Fig. 1). Isotopomer measurements provide information on carbon-carbon connectivities in metabolites, in systems supplied with a mixture of U-^{13}C-labeled and U-^{12}C-labeled substrates (Szyperski, 1995, 1998). Therefore, isotopomer abundance data facilitate statistically superior estimation of metabolic fluxes and reaction reversibilities than atom enrichment data (Wiechert et al., 1999). The second important development in flux quantification in plants was by Ohlrogge and co-workers, who used mass isotopomer data of metabolites separated from developing *Brassica napus* embryos to calculate fluxes (Schwender et al., 2003), although only the glycolysis and oxPPP were considered.

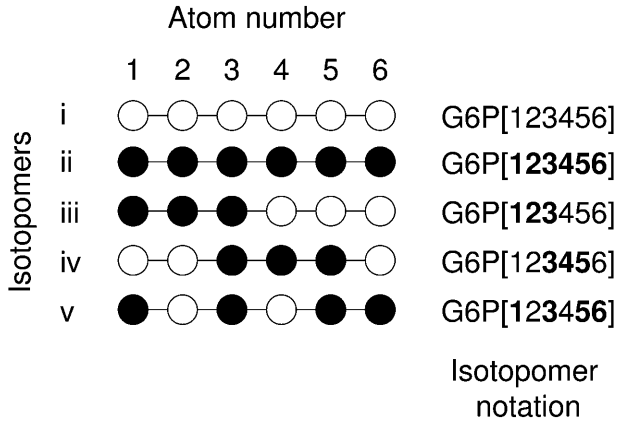

Figure 1. Isotopomers (isotope isomers) of a metabolite. Five isomers (i–v) of the six-carbon metabolite G6P are shown. These isomers differ in the labeling state (^{13}C or ^{12}C) of their individual carbon atoms. Here, ^{13}C atoms are depicted as black circles, and ^{12}C atoms are depicted as white circles. Isotopomers are notated using boldface for ^{13}C and regular font for ^{12}C, as illustrated on the on the right of each isotopomer. A metabolite with n carbon atoms has 2^n isotopomers but only n ^{13}C atom enrichment measurements. Therefore, isotopomer measurements usually provide superior information about the labeling state of a metabolite, compared to ^{13}C atom enrichments.

Despite these advances, flux measurement in plants is in its early stages. Systemic evaluation of fluxes from overdetermined isotopomer data sets as well as detailed statistical analysis of the evaluated fluxes have not yet been implemented in plant metabolism to the extent of their application to prokaryotic metabolism. Second, the quantification of fluxes of parallel pathways in two compartments (e.g. cytosolic and plastidic oxPPP, mitochondrial and plastidic malic enzymes) has not been reported to date. Also, while the aforementioned studies have isolated metabolites before collecting labeling data, this effort-intensive step is not necessary since two-dimensional (2-D) NMR can be used to resolve a mixture of several metabolites.

In this article, we report labeling studies and flux quantification in developing embryos of soybean (*Glycine max*), metabolizing Suc and Gln in liquid culture. Soybeans are important sources of protein, oil, and nutraceuticals, and developing embryos are important in vitro model systems to study them (Saravitz and Raper, 1995). There exists motivation to physiologically characterize this system to understand carbon partitioning between pathways and identify potential metabolic engineering targets. We acquired an overdetermined isotopomer abundance data set in a high-throughput fashion, using 2-D NMR. To convert the isotopomer abundances in this data set to fluxes, a computer tool was developed, which incorporated recent mathematical and statistical advances (Wiechert et al., 1999; Sriram and Shanks, 2001, 2004; Wiechert and Wurzel, 2001) in metabolic flux analysis theory. This tool is not specific to our metabolic network model and accepts user-defined metabolic models. Our results show that in the developing embryos, large amounts of carbon are shunted through the oxPPP and through the gluconeogenic pathway from triose phosphate to Fru phosphate in the plastid. The activities of the anaplerotic pathways, glyoxylate shunt, and γ-aminobutyric acid (GABA) shunt were also quantified. Moreover, we were able to distinguish between parallel pathways in separate compartments.

RESULTS

We performed labeling experiments by culturing developing soybean embryos in liquid medium with

Suc (10% [w/w] U-^{13}C, 90% [w/w] naturally abundant) and Gln (naturally abundant) as the only carbon sources. This labeling technique is termed biosynthetically directed fractional ^{13}C labeling (Szyperski, 1995). After 6 d of culture, a protein fraction and a starch fraction were extracted from the embryos and hydrolyzed. Then 2-D NMR experiments were performed on the respective hydrolysates, and heteronuclear [^{13}C, ^{1}H]-type NMR spectra were acquired. These spectra were used to quantify isotopomeric compositions of sink metabolites.

2-D NMR [^{13}C, ^{1}H] Spectra of Sink Metabolites and Cross-Peak Assignments

A [^{13}C, ^{1}H] heteronuclear single quantum correlation (HSQC) spectrum of the seed protein hydrolysate is shown in Figure 2. The ^{13}C axis (labeled F1) on this spectrum spans the ^{13}C chemical shift range 10 to 50 parts per million (ppm). Cross-peaks on this spectrum correspond to carbon atoms (that are attached to protons) of compounds in the protein hydrolysate. In the spectrum shown in Figure 2, we identified aliphatic carbon atoms of 16 amino acids, levulinic acid (LVA), and 5-hydroxymethyl furfural (HMF). Each carbon atom was identifiable by its unique ^{13}C and ^{1}H chemical shifts as well as distinctive coupling patterns and J-coupling constants (J_{CC}). Explanations of chemical shifts and J_{CC} are provided by Harris (1983).

The amino acids identified in the spectrum resulted from degradation of the seed protein under the hydrolysis conditions employed (145°C, vacuum, 6 N HCl) and are therefore proteinogenic amino acids synthesized in the embryos. The LVA and HMF peaks appear on the spectrum because soybean seed storage protein (most of the protein in the developing embryo) is highly glycosylated (Doyle et al., 1986), the attached sugars being predominantly Man and glucosamine (Yamauchi and Yamagishi, 1979). Under the hydrolysis conditions employed, the hexose skeletons of Man, Glc, and glucosamine are converted to LVA and HMF (G. Sriram, V.V. Iyer, and J.V. Shanks, unpublished data).

To assign the cross-peaks to carbon atoms, chemical shift values for the amino acids obtained from Wüthrich et al. (1976) and J_{CC} values obtained from Krivdin and Kalabin (1989) were used. The assignments were also verified using supplementary 2-D and 3-D NMR spectra of the hydrolysate of a 100% ^{13}C-labeled protein (data not shown). Chemical shifts and J_{CC} values for the carbon atoms of LVA and HMF were obtained by analyzing [^{13}C, ^{1}H] spectra of hydrolysates of Glc labeled at various positions (G. Sriram, V.V. Iyer, and J.V. Shanks, unpublished data).

A second [^{13}C, ^{1}H] HSQC spectrum of the seed storage protein was acquired, where the ^{13}C axis spanned the chemical shift range 90 to 160 ppm. Herein, the aromatic carbon atoms of Tyr, Phe, and His were detected. A [^{13}C, ^{1}H] spectrum of the starch hydrolysate was acquired, where the ^{13}C axis spanned the chemical shift range 10 to 50 ppm. This spectrum contained peaks corresponding to the aliphatic carbon atoms of LVA and HMF. This is expected since starch is

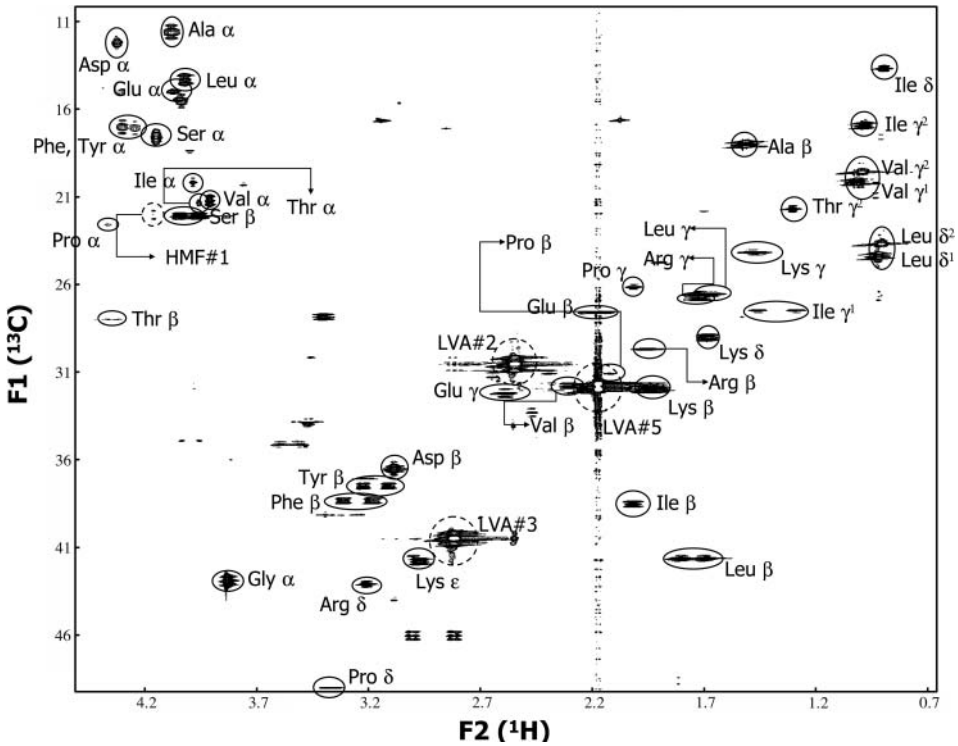

Figure 2. Two-dimensional [^{13}C, ^{1}H] HSQC spectrum of protein hydrolysate. Protein was isolated from soybean cotyledons cultured on Suc (10% [w/w] U-^{13}C) and Gln. Cross-peaks represent carbon atoms of hydrolysate constituents (proteinogenic amino acids, HMF, LVA). The names of some amino acid nuclei are omitted for clarity.

a Glc polymer, and its hydrolysate should contain LVA and HMF for the reasons stated above.

Fine Structures of Peaks and Quantification of Isotopomer Abundances

The cross-peaks in the [^{13}C, ^{1}H] spectrum displayed peak splitting along the ^{13}C dimension, due to ^{13}C-^{13}C scalar coupling, as is evident in expanded views of the cross-peaks, e.g. Gly α and Asp β (Fig. 3). Detailed descriptions of scalar coupling, why it causes peak splitting, and the types of satellite peaks resulting from peak splitting, are provided by Harris (1983) and Cavanagh et al. (1996). Briefly, such peak splitting indicates the presence of multiple isotopomers of the detected compounds. For instance, the Gly α-peak exhibits a central singlet peak (s) and two doublet peaks (d) distributed on either side of the singlet (Fig. 3A). The singlet in the Gly α fine structure represents a population of Gly isotopomers in which the α-atom (α) has a ^{13}C nucleus, and the carboxyl atom (C) adjacent to it has a ^{12}C nucleus. Whereas, the doublet represents a population of Gly isotopomers in which the α-atom and the carboxyl atom both have ^{13}C nuclei. Using boldface to represent ^{13}C atoms and regular font for ^{12}C atoms, the isotopomer population corresponding to the singlet may be represented as [C**α**], and the one corresponding to the doublet as [**Cα**]. Likewise, the fine structure of the Asp β cross-peak shows a singlet (s), a doublet (d1), a doublet (d2), and a double doublet (dd; Fig. 3B). As per the above notation, the isotopomer population represented by the singlet is [xα**β**γ], that represented by the doublet d1 is [x**αβ**γ], that by the doublet d2 is [xα**βγ**], and that by the double doublet is [x**αβγ**]. Here, x stands for an undeterminable labeling state, i.e. the atom represented by x (Asp carboxyl) cannot be detected from the Asp β fine structure.

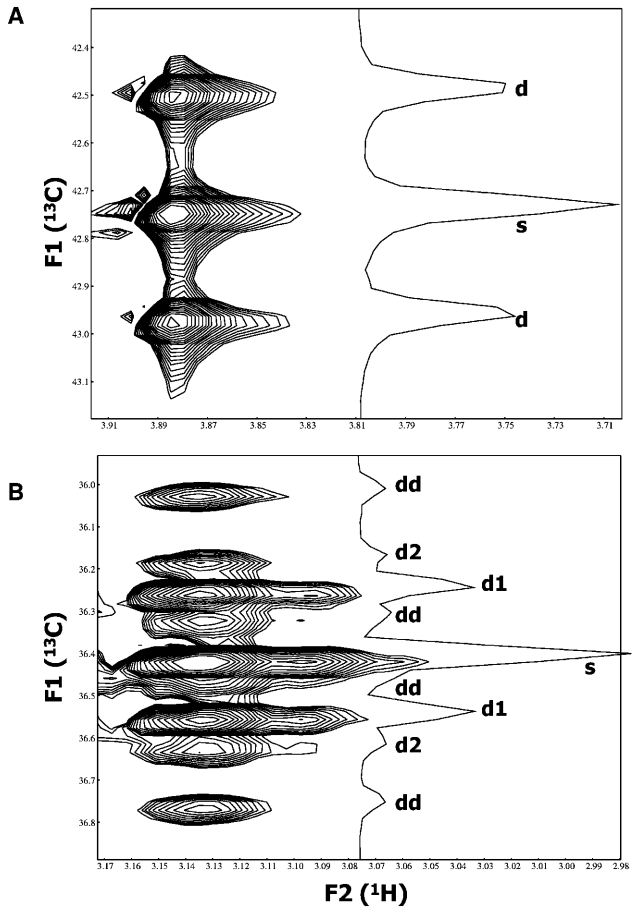

Figure 3. Expanded views of [^{13}C, ^{1}H] HSQC spectrum: Gly α (A) and Asp β (B) cross-peaks. One-dimensional slices are shown alongside. The multiplet peaks are: s, singlet; d, d1, d2, doublet; dd, double doublet.

These satellite peaks observed in the fine structure of a given cross-peak are termed multiplets. The abundances of the isotopomer populations represented by the multiplets are directly proportional to the integrals of the respective multiplet peaks. We quantified peak integrals by various methods depending on the complexity of the fine structure, as described in ''Materials and Methods.'' The isotopomeric compositions of sink metabolites resulting from the quantification (a total of 155 relative isotopomer abundances) are listed in Supplemental Material I.

Labeling States of Precursor Metabolites by Retrobiosynthetic Analysis

To evaluate metabolic fluxes of reactions in primary metabolism, the isotopomer abundances of central metabolic precursors need to be calculated. These were determined from the labeling states of the sink metabolites by retrobiosynthetic reconstruction, following the approach of Szyperski (1995) and Glawischnig et al. (2001). For instance, Thr is metabolically synthesized from its precursor, plastidic oxaloacetate (OAA^{P}), and the four carbon atoms of Thr (denoted as [C$\alpha\beta\gamma$]) correspond to the carbon atoms of OAA^{P} (denoted as [1234]). Since OAA^{P} is the only source of Thr, its isotopomeric composition should be calculable from that of Thr. For example, the fractional abundance of the OAA isotopomer [12**3**x] (relative to the total OAA pool) should be equal to that of the Thr isotopomer [C**α**βx] or the intensity of the singlet in the Thr α peak (relative to the total Thr α signal). The precursor isotopomer structures corresponding to the quantified multiplets are shown in Supplemental Material I. In some cases, only sums of isotopomers can be assigned to a multiplet, rather than a single isotopomer. This occurs for cross-peaks such as Tyr β, where the doublet represents the sum of two Tyr isotopomers. It also occurs for cross-peaks of sink metabolites that are synthesized from multiple metabolic precursors, such as Lys, which is synthesized from pyruvate and OAA.

The multiplet intensities of the sink metabolites provide an overdetermined data set for the calculation of the isotopomeric compositions of their precursor. This is because, usually, multiple sink metabolites are

synthesized from the same metabolic precursor. For example, plastidic phospho*enol*pyruvate (PEP^P) is a metabolic precursor to both Phe and Tyr. The abundance of the PEP^P isotopomer [1**2**3] determined from the Phe α singlet was 0.205 $\pm$ 0.012, while that determined from the Tyr α singlet was 0.208 $\pm$ 0.017. Both values are in close agreement. Good consistency was noted for all amino acids synthesized from the same precursor. Leu δ^1 was found to be the only exception. When the abundance of the isotopomer [x**23**] of plastidic pyruvate (Pyr^P) was determined from the singlets of three amino acids synthesized from Pyr^P (Leu δ^1, Val γ^1, and Ile γ^2), the values obtained from Val γ^1 (0.235 $\pm$ 0.002) and Ile γ^2 (0.242 $\pm$ 0.002) were in agreement with each other and with the abundance of the same isotopomer [x**23**] of PEP^P, the immediate precursor of Pyr. However, the value obtained from Leu δ^1 (0.357 $\pm$ 0.005) is significantly different.

Isotopic Equilibration of Metabolites between Compartments

We observed that the isotopomeric compositions of two hexose nucleotide pools—one located in the cytosol and another in the plastid—were dissimilar. These were obtained from the LVA and HMF peaks of the protein and starch hydrolysates. Starch, a Glc polymer, is synthesized from plastidic ADP-Glc, which is in isotopic equilibrium with the hexose nucleotides in the plastid. Therefore, the isotopomeric composition of the Glc monomer of starch (obtained from its hydrolysis products LVA and HMF) reflects the isotopomeric composition of the plastidic hexose nucleotide pool. On the contrary, the hexose sugars attached to glycosylated protein are synthesized from nucleotide sugars UDP-Glc or GDP-Man (Faik et al., 2000; Baldwin et al., 2001), the synthesis of which occurs in the cytosol (Coates et al., 1980). Therefore, the isotopomeric composition of the cytosolic hexose nucleotide pool is determinable from the LVA and HMF peaks in the protein hydrolysate spectrum. Figure 4A shows a comparison of the isotopomer abundances of the cytosolic and plastidic hexose nucleotide pools determined thus. Clearly, most of the abundances are significantly different. This suggests the presence of separate, nonequilibrating metabolic pathways in the cytosol and the plastid.

However, the isotopomeric compositions of the triose phosphates in cytosolic and plastidic compartments were not significantly different. These were obtained by comparing the multiplet intensities of Ala α, Phe α, and Tyr α. Phe and Tyr are synthesized from plastidic PEP and therefore reflect the isotopomeric composition of the plastidic triose phosphates. Ala is synthesized both in the cytosol and in the plastid (Ireland and Lea, 1999); therefore, its isotopomeric composition represents a combination of those of the triose phosphates in both compartments. From Figure 4B it is evident that corresponding isotopomer abundances are similar. However, the multiplet intensities

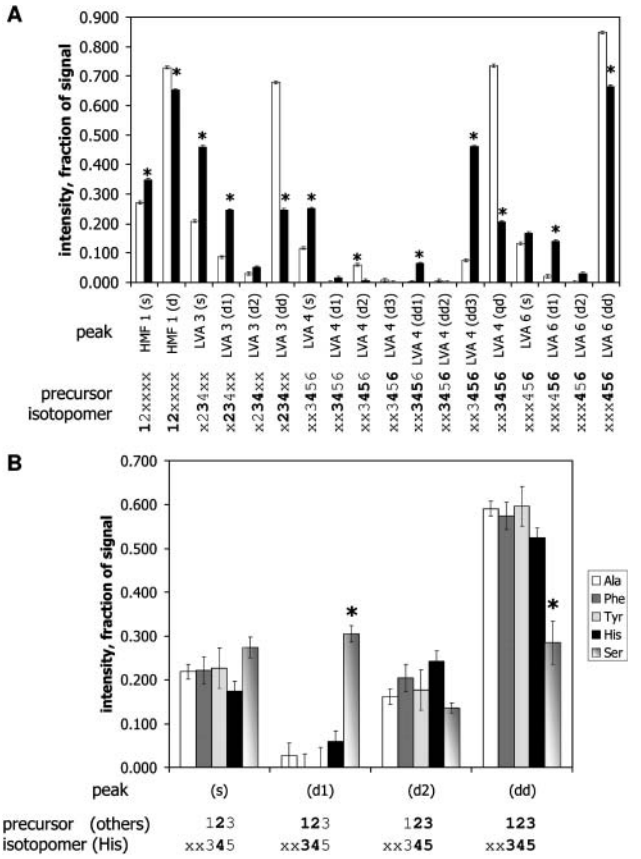

Figure 4. A, Comparison of corresponding multiplet intensities of LVA and 5-HMF from [^{13}C, ^{1}H] spectra of protein (white bars) and starch (black bars) hydrolysates. Each peak represents an isotopomer of the cytosolic (protein hydrolysate) or the plastidic (starch hydrolysate) hexose nucleotide pool. (See "Results" for details.) These precursor isotopomers are shown next to the *x* axis, following the notation introduced in Figure 1 and "Results." Starch hydrolysate multiplets whose multiplet intensities are significantly different from the corresponding protein hydrolysate multiplets are marked with an asterisk (*). B, Comparison of corresponding multiplet intensities of Ala α, Phe α, Tyr α, Ser α, and His α cross-peaks. The isotopomeric compositions of the precursors of the amino acids are shown next to the *x* axis. Ser multiplets, whose multiplet intensities are significantly different from the mean of the other multiplets, are marked with an asterisk (*).

of Ser α (doublet d1 and double doublet) are different. This suggests the involvement of Ser in reactions in which the triose phosphate pool (T3P) does not participate.

Interestingly, the multiplet intensities of His α, which represents the isotopomers of the [xx345] fragment of plastidic pentose phosphate, $P5P^P$, bear similarity with the multiplets of Ala α, Phe α, and Tyr α. This suggests rapid equilibration between $P5P^P$ and the T3P pool represented by Ala α, Phe α, and Tyr α. $P5P^P$ and $T3P^P$ are interconverted by the transketolase reaction, a highly reversible reaction of the nonoxidative limb of the oxPPP (Lea and Leegood, 1999). The presence of transketolase in the plastid is therefore implied.

The Carbon in Pyr^p Originates Largely from Suc

We found that the carbon in Pyr^p originates almost entirely from Suc and not from other external carbon substrates Gln or CO_2. The carbon in any metabolite synthesized in the embryos could be a mixture of the carbon from three available external carbon sources: Suc, Gln (both present in the liquid medium), or CO_2 (through photosynthetic fixation). To determine the contributions of these carbon sources to the carbon in Pyr^p, we determined the ^{13}C enrichment of atom 3 of Pyr^p and compared it with the ^{13}C enrichment of the carbon sources. The doublet intensities of Leu δ^2 and Val γ^2 provide the ^{13}C enrichment of atom 3 of Pyr^p synthesized de novo since the beginning of the labeling experiment (Szyperski, 1995). In our data, these intensities were: Leu $\delta^2(d) = 0.123 \pm 0.001$ and Val $\gamma^2(d) = 0.118 \pm 0.002$. Among the three external carbon sources, Suc had a substantial ^{13}C enrichment in the range 0.11 to 0.12 (i.e. 0.10 from U-^{13}C Suc and approximately 0.011 from natural ^{13}C abundance), while Gln and CO_2 had a small natural ^{13}C abundance of 0.011.

Thus, the ^{13}C enrichment of Pyr^p synthesized during the labeling experiment was almost identical to the ^{13}C enrichment of the substrate Suc and significantly different from the enrichments of the substrates Gln or CO_2. This observation implies that the carbon in Pyr^p originates entirely from the Suc in the medium. Therefore, the Gln in the medium or external CO_2 fixation by photosynthesis make small or negligible contributions to the carbon in Pyr^p, since a substantial contribution from either of these carbon sources to Pyr^p would have resulted in its ^{13}C enrichment being considerably lower than 0.11.

Extracellular Fluxes and Fluxes Contributing to Biomass Accumulation

The measurements of extracellular fluxes and fluxes toward biomass synthesis were as follows. The average rate of biomass accumulation in the developing soybean embryos was 2.3 g d^{-1} $cotyledon^{-1}$. The Suc consumption was 9.59×10^{-6} μmol d^{-1} $cotyledon^{-1}$. The contents of biomass, including protein, oil, starch, and proteinogenic amino acid proportions, are listed in Supplemental Material II. The proportions of amino acids in the protein compared well with published values for soybean embryo seed storage protein (Bewley and Black, 1994).

Metabolic Network Model

The calculation of metabolic fluxes from labeling data requires a model of the metabolic network. Our model is shown in Figure 5. It includes all principal pathways of primary metabolism (glycolysis, oxPPP, TCA cycle, anaplerotic shunts, glyoxylate shunt, and GABA shunt) and the biosynthetic pathways that convert the primary metabolic precursors to sink metabolites. Also, it includes three metabolic compartments: cytosol, plastid, and mitochondrion. The pathways in the model were assigned to specific compartments based on information in the current literature (see references below). Some pathways could not be unequivocally assigned to a single compartment, since they are known to operate separately in multiple compartments. Thus, we included separate glycolysis and oxPPP pathways in the cytosol and plastid, as well as separate malic enzyme (Mal → Pyr) fluxes in the plastid and mitochondrion.

The sources of information for the primary metabolic and biosynthetic pathways in the model were the recent literature on soybean embryo or higher plant biochemistry (Breitkreuz and Shelp, 1995; Chollet et al., 1996; Lam et al., 1996; Casati et al., 1999; Hermann and Weaver, 1999; Singh, 1999; Drincovich et al., 2001; Jeanneau et al., 2002), plant biochemistry texts (Dey and Harborne, 1997; Lea and Leegood, 1999), and the online catalog Soybase (2004). These sources also provided information on the precursors of the sink metabolites. Stoichiometries and carbon atom rearrangements for the reactions were obtained from the Kyoto Encyclopedia of Genes and Genomes (KEGG, 2004).

The reactions in the model were assumed reversible unless information on irreversibility was available. All reversible reactions were modeled as two fluxes (see Supplemental Material IV, p. 10). The reaction from succinate to malate (Mal) in the TCA cycle can lead to an inversion of the labeling pattern, owing to the fact that succinate is a symmetrical molecule while Mal is not (Schmidt et al., 1999). To account for this fact, this reaction was modeled as two parallel fluxes, one that conserves the carbon skeleton and another that inverts the same (see Supplemental Material IV, p. 10).

The metabolic model also incorporated the observations reported in the previous sections. Specifically, the photosynthetic reactions (Calvin cycle) were not included in our model because carbon assimilation by external CO_2 fixation was found to be negligible. Because differences were observed between the isotopomeric compositions of the cytosolic and plastidic hexose nucleotide pools, we assumed separate glycolysis pathways and oxPPPs to operate in those compartments, with the cytosolic and plastidic G6P pools acting as precursors to the respective hexose nucleotide pools. To account for the difference in the isotopomeric compositions of Ser and T3P, we incorporated a reversible reaction between Ser and Gly, which is known to occur during the catabolism of Ser in heterotrophic plant tissues (Bourguignon et al., 1999).

Metabolic Fluxes

Fluxes in the above metabolic network were calculated from the measured isotopomer abundances, extracellular fluxes, and biomass composition by using a flux evaluation mathematical routine that incorporated isotopomer balancing and global optimization.

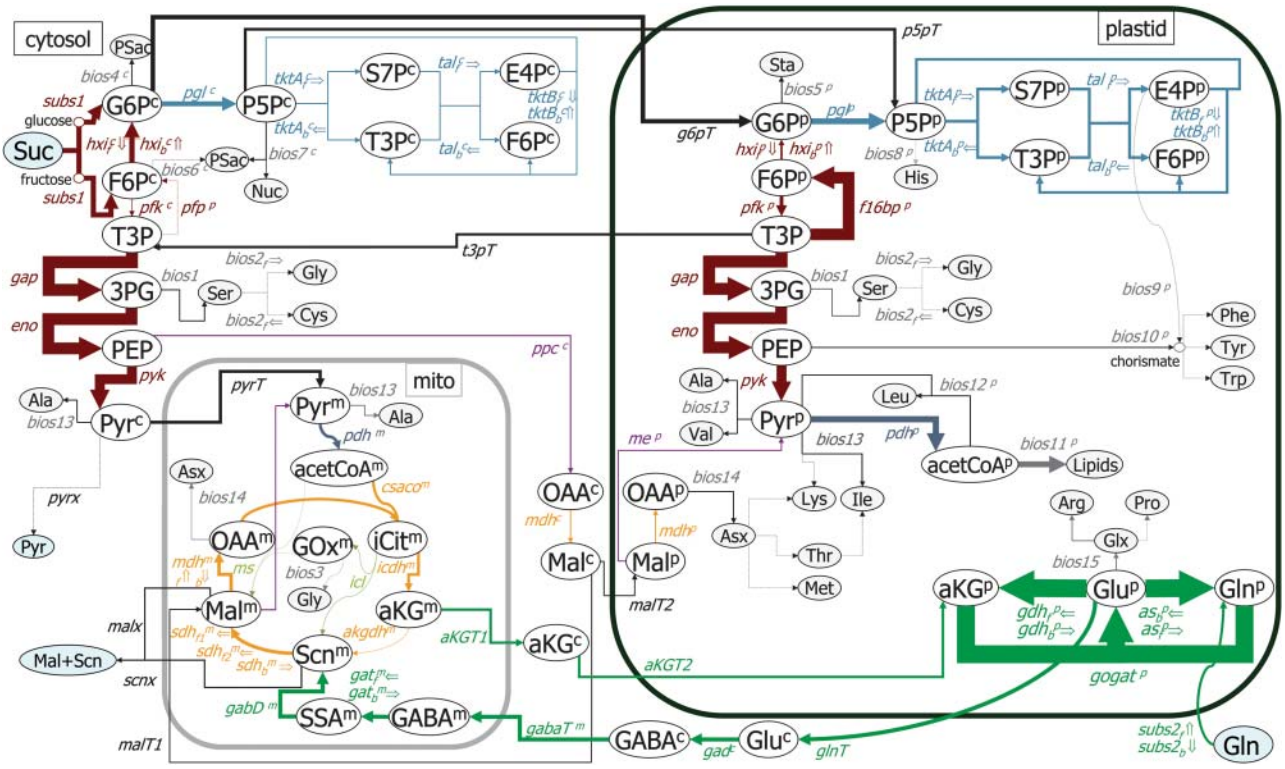

Figure 5. Metabolic flux map of primary and intermediate metabolic pathways in developing soybean cotyledons cultured on Suc (10% [w/w] U-^{13}C) and Gln. Fluxes are proportional to arrow widths. (Fluxes less than 0.4 μmol d^{-1} cotyledon^{-1} are shown with lines of lowest visible thickness.) Arrows indicate the direction of net flux. A complete numerical listing of estimated flux values and reaction reversibilities is provided in Figure 6. Intracellular metabolites are shown in white ovals, and gray ovals show sink metabolites (proteinogenic amino acids, polysaccharides, etc.). Metabolites taken up from/secreted into the medium are shown in blue ovals. Metabolic pathways are color coded as follows: dark red, glycolysis and Suc metabolism; pale blue, pentose phosphate pathway; orange, TCA cycle; blue-gray, pyruvate dehydrogenase link; mauve, anaplerotic fluxes; dark yellow, glyoxylate shunt; green, Glu metabolism, GABA shunt, and associated intercompartmental transport fluxes; gray, fluxes toward biomass synthesis; and black, all intercompartmental transport fluxes except those involved in Gln metabolism and GABA shunt. Abbreviations for intracellular metabolites not defined in the text are as follows: P5P, pentose-5-P; S7P, sedoheptulose-7-P; E4P, erythrose-4-P; acetCoA, acetyl CoA; iCit, isocitrate; aKG, α-ketoglutarate; Scn, succinate; SSA, succinic semi-aldehyde; and GOx, glyoxylate. Sink metabolite abbreviations are as follows: Psac, polysaccharides; Nuc, carbon skeleton of nucleotides; and Sta, starch. Asp and Asn are denoted together as Asx. Glu and Gln are denoted together as Glx. F6P and T3P appear at two different locations each in the cytosol and plastid, to avoid confusing intersections of lines. Each flux is assigned a short name based on the name of the gene encoding one of the metabolic reactions represented by it. Intracellular metabolites and fluxes with a superscript are located in specific subcellular compartments: c, cytosol; p, plastid; and m, mitochondrion. If a flux has no superscript, its compartmentation could not be unambiguously determined (such as *gap*, *eno*, and *pyk*, and some fluxes toward biosynthesis).

(All mathematical and computational details are explained in Supplemental Material IV–VI.) The objective of this routine was to evaluate a set of stoichiometrically feasible fluxes that best accounts for the isotopomer and extracellular flux measurements. The flux evaluation routine was implemented by a computer program, NMR2Flux. It was ensured that the iteratively evaluated flux solution is unique by repeating the flux evaluation at least 300 times from arbitrary starting points. SD for the fluxes and reversibility extents were computed from a statistical analysis. (For details, see Supplemental Material IV, p. 21.)

The evaluated fluxes are listed in Figure 6 and also depicted in Figure 5 (arrow widths in this figure are directly proportional to flux). Figure 7 depicts the agreement between experimental multiplet intensities and those simulated from the evaluated fluxes. It can be seen that the evaluated fluxes explain the labeling data well. Only a few outlier points can be observed, of which the Leu δ^1 intensities (shown with black circles) were the largest contributors to the cumulative χ^2 error between the simulated and experimental intensities.

The flux into the oxPPP was found to be 9.10 $\pm$ 3.85 μmol d^{-1} cotyledon^{-1} in the cytosol and 10.90 $\pm$ 4.97 μmol d^{-1} cotyledon^{-1} in the plastid, the total flux being 19.99 $\pm$ 4.39 μmol d^{-1} cotyledon^{-1}. On a carbon mole basis, this is 104.2 carbon mol $\pm$23.0 carbon mol per 100 carbon mol of Suc uptake. Also, the flux of the hexose phosphate isomerase reaction, in both the cytosol and plastid, is in the direction Fru-6-P

	Reaction name	Stoichiometry	Net flux		Reversibility		Comment
			Mean	SD	Mean	SD	
	Glycolysis and oxPPP						
{	hxi_f^c	$G6P^c \rightarrow F6P^c$	-9.56	1.52	51.8	26.7	Flux is in the direction $F6P^c \rightarrow G6P^c$
{	hxi_b^c	$F6P^c \rightarrow G6P^c$					
{	hxi_f^p	$G6P^p \rightarrow F6P^p$	-3.66	4.23	97.0	3.2	Flux is in the direction $F6P^p \rightarrow G6P^p$
{	hxi_b^p	$F6P^p \rightarrow G6P^p$					
	hxi_f	$G6P \rightarrow F6P$	-13.22	4.83	—	—	Combined *hxi* flux (cytosol+plastid)
	pgl^c	$G6P^c \rightarrow P5P^c + CO_2$	9.10	3.85	irrev.	—	
	pgl^p	$G6P^p \rightarrow P5P^p + CO_2$	10.90	4.97	irrev.	—	
	pgl	$G6P^c \rightarrow P5P + CO_2$	19.99	4.39	irrev.	—	Combined *pgl* flux (cytosol+plastid)
{	$tktA_f^c$	$P5P^c + P5P^c \rightarrow S7P^c + T3P^c$	0.61	0.25	90.4	17.9	
{	$tktA_b^c$	$S7P^c + T3P^c \rightarrow P5P^c + P5P^c$					
{	$tktA_f^p$	$P5P^p + P5P^p \rightarrow S7P^p + T3P^p$	5.45	1.50	88.5	14.6	
{	$tktA_b^p$	$S7P^p + T3P^p \rightarrow P5P^p + P5P^p$					
{	tal_f^c	$S7P^c + T3P^c \rightarrow F6P^c + E4P^c$	0.61	0.25	46.7	25.1	
{	tal_b^c	$F6P^c + E4P^c \rightarrow S7P + T3P^c$					
{	tal_f^p	$S7P^p + T3P^p \rightarrow F6P^p + E4P^p$	5.45	1.50	76.2	16.1	
{	tal_b^p	$F6P^p + E4P^p \rightarrow S7P^p + T3P^p$					
{	$tktB_f^c$	$P5P^c + E4P^c \rightarrow F6P^c + T3P^c$	0.61	0.25	6.7	10.9	
{	$tktB_b^c$	$F6P^c + T3P^c \rightarrow P5P^c + E4P^c$					
{	$tktB_f^p$	$P5P^p + E4P^p \rightarrow F6P^p + T3P^p$	5.08	1.50	34.2	30.7	
{	$tktB_b^p$	$F6P^p + T3P^p \rightarrow P5P^p + E4P^p$					
	pfk^c	$F6P^c \rightarrow T3P^c + T3P^c$	1.21	1.46	irrev.	—	
	pfk^p	$F6P^p \rightarrow T3P^p + T3P^p$	6.86	1.74	irrev.	—	
	pfk	$F6P \rightarrow T3P + T3P$	8.07	1.43	irrev.	—	Combined *pfk* flux (cytosol+plastid)
	pfp^c	$T3P^c + T3P^c \rightarrow F6P^c$	0.31	0.36	irrev.	—	
	$f16bp^p$	$T3P^p + T3P^p \rightarrow F6P^p$	21.72	5.00	irrev.	—	
	gap	$T3P \rightarrow 3PG$	22.55	1.42	n. d.	—	For *gap*, *eno* and *pyk*, cytosolic and
	eno	$3PG \rightarrow PEP$	21.38	1.42	n. d.	—	plastidic fluxes are indistinguishable. There-
	pyk	$PEP \rightarrow Pyr$	18.50	1.13	n. d.	—	fore, only combined fluxes are reported.
	pdh^p	$Pyr^p \rightarrow ACA^p + CO_2$	11.47	<0.08	irrev.	—	
	pdh^m	$Pyr^m \rightarrow ACA^m + CO_2$	5.59	1.35	irrev.	—	
	$pyrT$	$Pyr^c \rightarrow Pyr^m$	5.59	1.35	n. d.	—	
{	$g6pT_f$	$G6P^c \rightarrow G6P^p$	8.07	3.85	50.2	26.7	
{	$g6pT_b$	$G6P^p \rightarrow G6P^c$					
{	$t3pT_f$	$T3P^c \rightarrow T3P^p$	-4.41	2.88	96.2	6.6	Flux is in the direction $T3P^p \rightarrow T3P^c$
{	$t3pT_b$	$T3P^p \rightarrow T3P^c$					
{	$p5pT_f$	$P5P^c \rightarrow P5P^p$	5.19	3.97	75.4	28.3	
{	$p5pT_b$	$P5P^p \rightarrow P5P^c$					
	TCA cycle						
	$csaco^m$	$ACA^m + OAA^m \rightarrow ICit^m$	5.11	1.33	irrev.	—	Lumped flux, citrate synthase+aconitase
	$icdh^m$	$ICit^m \rightarrow aKG^m + CO_2$	4.64	1.33	irrev.	—	
	$akgdh^m$	$aKG^m \rightarrow Scn^m + CO_2$	0.60	1.96	irrev.	—	Confidence interval is [0.0, 2.56]
	sdh_{f1}^m	$Scn^m \rightarrow Mal^m$	2.54	0.93			Two forward reactions are considered:
{	sdh_{f2}^m	$Scn^m \rightarrow Mal^m$	3.90	1.05	39.2	11.6	sdh_{f1}^m conserves orientation and
{	sdh_b^m	$Mal^m \rightarrow Scn^m$	—	—			sdh_{f2}^m inverts orientation of succinate
{	mdh_f^m	$Mal^m \rightarrow OAA^m$	6.34	1.35	45.1	31.8	
{	mdh_b^m	$OAA^m \rightarrow Mal^m$					
	Glyoxylate shunt						
	icl^m	$ICit^m \rightarrow GOx^m + Scn^m$	0.47	0.03	irrev.	—	
	ms^m	$ACA^m + GOx^m \rightarrow Mal^m$	0.00	0.02	irrev.	—	

Figure 6. (*Figure continues on following page.*)

	Reaction name	Stoichiometry	Net flux		Reversibility		Comment
			Mean	SD	Mean	SD	
Anaplerotic reactions							
	ppc^{c}	$PEP^{c} + CO_2 \rightarrow OAA^{c}$	2.12	0.31	irrev.	—	
	me^{m}	$Mal^{m} \rightarrow Pyr^{m} + CO_2$	0.90	0.41	irrev.	—	
	me^{p}	$Mal^{p} \rightarrow Pyr^{p} + CO_2$	0.57	0.25	irrev.	—	
GABA shunt							
	gad^{c}	$Glu^{c} \rightarrow GABA^{c} + CO_2$	7.68	2.18	irrev.	—	
	gabaT	$GABA^{c} \rightarrow GABA^{m}$	7.68	2.18	n. d.	—	
{	*gat*$_f$^{m}	$GABA^{m} \rightarrow SSA^{m}$	7.68	2.18	49.4	32.9	
{	*gat*$_b$^{m}	$SSA^{m} \rightarrow GABA^{m}$	0.00	0.00			
	ssadh^{m}	$SSA^{m} \rightarrow Scn^{m}$	7.68	2.18	n. d.	—	
Substrate entry							
	subs1	$Suc^{ext} \rightarrow G6P^{c} + F6P^{c}$	9.59	0.10	n. d.	—	
{	*subs2*$_f$	$Gln^{ext} \rightarrow Gln^{c}$	4.76	0.23	23.6	3.4	
{	*subs2*$_b$	$Gln^{c} \rightarrow Gln^{ext}$	0.00	0.00			
Glutamate assimilation							
	glnT	$Gln^{c} \rightarrow Gln^{p}$	4.76	0.23	n. d.	—	
	aKGT1	$aKG^{m} \rightarrow aKG^{c}$	4.76	0.23	n. d.	—	
	aKGT2	$aKG^{c} \rightarrow aKG^{p}$	4.76	0.23	n. d.	—	
	gogatp	$aKG^{p} + Gln^{p} \rightarrow Glu^{p} + Glu^{p}$	88.52	43.83	irrev.	—	
{	*gdhfp*	$Glu^{p} \rightarrow aKG^{p}$	83.94	43.83	99.0	< 1.0	
{	*gdhbp*	$aKG^{p} \rightarrow Glu^{p}$	0.00	0.00			
{	*asf*	$Glu^{p} \rightarrow Gln^{p}$	83.68	43.84	61.0	28.1	
{	*asb*	$Gln^{p} \rightarrow Glu^{p}$	0.00	0.00			
Malate shuttle							
{	*malT1*$_f$	$Mal^{m} \rightarrow Mal^{c}$	-0.80	0.44	96.5	1.5	Flux is in the direction $Mal^{C} \rightarrow Mal^{m}$
{	*malT1*$_b$	$Mal^{c} \rightarrow Mal^{m}$	0.00	0.00			
	malT2	$Mal^{c} \rightarrow Mal^{p}$	1.32	0.44	n. d.	—	
	mdh^{c}	$Mal^{c} \rightarrow OAA^{c}$	-2.12	0.31	n. d.	—	Flux is in the direction $OAA^{C} \rightarrow Mal^{c}$
	mdh^{p}	$Mal^{p} \rightarrow OAA^{p}$	0.75	<0.08	n. d.	—	
Biosynthesis of Ser and Gly							
	bios1	$3PG \rightarrow Ser$	1.17	<0.08	irrev.	—	Biosynthesis of Ser
{	*bios2f*	$Ser \rightarrow Gly + C1$	0.45	0.24	46.4	1.2	Biosynthesis of Gly from Ser
{	*bios2b*	$Gly + C1 \rightarrow Ser$	0.00	0.00			
	bios3	$GOx \rightarrow Gly$	0.46	0.24	irrev.	—	Biosynthesis of Gly from glyoxylate
Fluxes towards biosynthesis (other than those related to Ser and Gly) and effluxes into medium							
	resp	$CO_2 \rightarrow$	49.81	2.56	irrev.	—	CO_2 release
	bios4	$G6P^{c} \rightarrow$ biomass	1.99	0.29	irrev.	—	Biosynthesis of polysaccharides
	bios5	$G6P^{p} \rightarrow$ biomass	0.83	0.27	irrev.	—	Biosynthesis of starch
	bios6	$F6P^{c} \rightarrow$ biomass	0.03	0.03	irrev.	—	Biosynthesis of polysaccharides
	bios7	$P5P^{c} \rightarrow$ biomass	2.08	0.16	irrev.	—	Biosynthesis of polysaccharides, nucleotides
	bios8	$P5P^{p} \rightarrow$ biomass	0.12	<0.08	irrev.	—	Biosynthesis of His
	bios9	$E4P^{p} \rightarrow$ biomass	0.37	<0.08	irrev.	—	To shikimate pathway, Phe, Tyr
	bios10	$PEP^{p} \rightarrow$ biomass	0.74	<0.08	irrev.	—	To shikimate pathway, Phe, Tyr
	bios11	$ACA^{p} \rightarrow$ biomass	10.95	<0.08	irrev.	—	Biosynthesis of fatty acids
	bios12	$ACA^{p} \rightarrow$ biomass	0.53	<0.08	irrev.	—	Biosynthesis of Leu
	bios13	$Pyr \rightarrow$ biomass	2.76	<0.08	irrev.	—	Biosynthesis of Val, Leu, Ala, Ile, Lys
	bios14	$OAA \rightarrow$ biomass	1.50	<0.08	irrev.	—	Biosynthesis of Asx, Ile, Thr, Met
	bios15	$Glu \rightarrow$ biomass	1.59	<0.08	irrev.	—	Biosynthesis of Pro, Arg, proteinogenic Glu
	pyrx	$Pyr \rightarrow$	0.17	0.12	irrev.	—	Efflux of Pyr into medium
	malx	$Mal \rightarrow$	2.32	0.53	irrev.	—	Combined efflux of Mal
	scnx	$Scn \rightarrow$	0.00	0.00	irrev.	—	and Scn into medium

Figure 6. (*Legend appears on following page.*)

(F6P) → Glc-6-P (G6P). This indicates that the glycolysis and oxPPP are operating in a cyclic manner, with the reverse hexose isomerase reaction feeding the oxPPP. Further, we were able to distinguish between the fluxes through the reversible nonoxidative limbs of the oxPPP in the cytosol and the plastid, which are catalyzed by transketolase and transaldolase. These fluxes were observed to be substantial in the plastid (5.45 ± 1.50 μmol d^{-1} $cotyledon^{-1}$) compared to the cytosol (0.61 ± 0.25 μmol d^{-1} $cotyledon^{-1}$). The flux from T3P to F6P was observed to be 21.72 ± 5.00 μmol d^{-1} $cotyledon^{-1}$ in the plastid and 0.31 ± 0.36 μmol d^{-1} $cotyledon^{-1}$ in the cytosol. The anaplerotic flux in the cytosol from PEP to OAA was observed to be 2.12 ± 0.31 μmol d^{-1} $cotyledon^{-1}$, while the reverse flux from Mal to Pyr was 0.90 ± 0.41 μmol d^{-1} $cotyledon^{-1}$ in the mitochondrion and 0.57 ± 0.25 μmol d^{-1} $cotyledon^{-1}$ in the plastid. The glyoxylate shunt flux was 0.47 ± 0.03 μmol d^{-1} $cotyledon^{-1}$ and, therefore, small compared to the TCA cycle flux (through citrate synthase and aconitase) of 5.11 ± 1.33 μmol d^{-1} $cotyledon^{-1}$. Most of the carbon in the TCA cycle appeared to be shunted through GABA (confidence limits: 5.50–9.86 μmol d^{-1} $cotyledon^{-1}$) rather than succinate thiokinase (confidence limits: 0.0–2.56 μmol d^{-1} $cotyledon^{-1}$). Also, the exchange fluxes between Gln, Glu, and α-ketoglutarate were found to be high.

Since our flux evaluation program, NMR2Flux, allowed alterations in the metabolic network model easily, many modifications to the initially assumed model were examined for their ability to accurately account for the labeling data. If a modification explained the data significantly better, it was accepted. Such posteriori changes to the model are the inclusion of the flux from T3P to F6P, which resulted in a 50% reduction in the χ^2 error, and the inclusion of an efflux into the medium from the succinate and Mal nodes in the TCA cycle. We included a reversible reaction between Ser and Gly to account for the observed isotopomeric difference between Ser and other glycolytic three-carbon units. A photorespiratory pathway was not required to account for this difference. The uptake of carbon from Gln had to be included to better account for the multiplet intensities of the amino acids of the Glu family and Asp/Asn. Also, an efflux from the Mal and succinate nodes of the TCA cycle was included. A contribution to Gly synthesis from glyoxylate was included, the calculated flux of which (0.46 ± 0.24 μmol d^{-1} $cotyledon^{-1}$) is comparable to that of the synthesis of Gly from 3-phosphoglycerate (3PG; 0.45 ± 0.24 μmol d^{-1} $cotyledon^{-1}$).

DISCUSSION

The use of steady-state isotope labeling methods is a reliable technique to quantify fluxes in metabolic pathways. Its use in plant metabolism began with the measurement of ^{13}C atom enrichments in tissues supplied with labeled substrate. The measurement of isotopomers (Glawischnig et al., 2000) was an important advance, since isotopomer abundances provide information on carbon-carbon connectivities (Szyperski, 1995, 1998) and, hence, an overdetermination of the labeling state compared to enrichments. However, the interpretation of observed isotopomer abundances has been largely qualitative or semiquantitative.

In this work, we calculated fluxes from overdetermined isotopomer abundance data. Fluxes are not explicit mathematical functions of the labeling data, particularly in elaborate metabolic networks involving metabolic cycles, reversible reactions, and compartmentation. Therefore, their evaluation from large isotopomer data sets is not trivial and requires advanced mathematical tools (Wiechert, 2001). To facilitate quick and efficient flux evaluation, we incorporated recent developments in efficient flux analysis such as automated isotopomer balancing and global optimization (for details, see Supplemental Material IV–VI). A computer program NMR2Flux that incorporated these methods was written to automatically evaluate fluxes from isotopomer abundance data and a metabolic network model.

Furthermore, the experimental methodology employed in this paper has the potential to become a high-throughput one because the employment of 2-D NMR obviated the need to physically separate the sink metabolites to measure their isotopomer abundances. Thus, the experimental load was considerably reduced. In previous research that reported ^{13}C labeling measurements of several metabolites from plants (Glawischnig et al., 2000; Rontein et al., 2002; Schwender et al., 2003), the detected metabolites were separated by chromatography. Besides, 2-D [^{13}C, ^{1}H] NMR enables the measurement of ^{13}C isotopomers with the high sensitivity of ^{1}H NMR rather than the relatively low sensitivity of ^{13}C NMR (Szyperski, 1998;

Figure 6. Metabolic fluxes evaluated for soybean embryos cultured on Suc (10% w/w U-^{13}C) and Gln. Absolute fluxes are expressed in μmol d^{-1} $cotyledon^{-1}$. Each flux is assigned a short name (usually based on the name of the gene encoding one of the metabolic reactions represented by the flux). Abbreviations for metabolites and color coding for fluxes is the same as in Figure 5. Fluxes grouped by left braces ({) are those of forward and backward reactions catalyzed by the same enzyme. (The forward and backward fluxes F6P → T3P and T3P → F6P are not grouped thus, since they are catalyzed by different enzymes.) For grouped fluxes, the net flux and reaction reversibility are shown. Net fluxes are in the direction of the reaction with the subscript f. Subscripts on reaction names are: f, forward reaction; and b, backward reaction. Superscripts are: c, cytosol; p, plastid; and m, mitochondrion. If a flux has no superscript, its compartmentation could not be unambiguously determined. Reversibilities are reported as percentages, with 0% = irreversible, 100% = reaction at equilibrium. irrev., Reaction assumed irreversible/known to be thermodynamically irreversible; n.d., reversibility of the reaction could not be determined as it was found to have negligible effect on the isotopomer abundances; SD, SD of flux or reversibility.

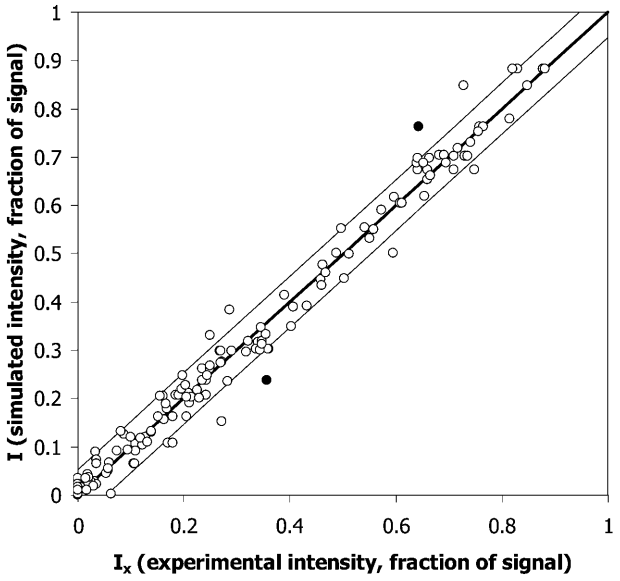

Figure 7. Comparison of experimental and simulated multiplet intensities, depicting how closely the evaluated fluxes account for the labeling data (multiplet intensities or isotopomer abundances). The *x* axis represents experimental multiplet intensities measured from [^{13}C, ^{1}H] spectra; the *y* axis represents relative intensities that were simulated by the computer program NMR2Flux, corresponding to the evaluated fluxes (Fig. 6). Multiplet intensities are shown as fraction of total signal. The thick diagonal line is the 45° diagonal, on which the error between measurement and simulation is zero. The thin lines enclose 90% of all data points (all points with error ≤0.0434). The singlet and doublet intensities of Leu δ^1 are shown as black circles.

Wiechert et al., 1999). The use of 2-D NMR is therefore crucial in the large-scale application of flux evaluation in plants.

The attainment of isotopic steady state is essential for the calculation of fluxes from the labeling data. For the in vitro soybean embryo culture employed here, the residence time of Suc in the cells is approximately 9.4 h, as calculated from the uptake of Suc (1.179×10^{-6} mol h^{-1} for three cotyledons) and the free-space Suc concentration documented for developing soybean embryos (37 mM; Lichtner and Spanswick, 1981). Isotopic steady state is attained within 5 residence times (i.e. <48 h or 2 d), which is less than the 6-d labeling period employed here. Therefore, the labeling data in this work can be assumed to be at steady state.

We observed that the measured isotopomer abundances of Leu δ^1 did not agree with the simulated abundances of its precursor, Pyr^P. However, all other amino acid atoms showed good agreement, including other amino acids synthesized from Pyr^P (Val γ^1, Ile γ^2). Also, the Leu δ^1 abundances were the largest contributors to the cumulative χ^2 error between simulated and experimental isotopomer abundances. We also found this anomaly in isotopomer data from soybean embryos cultured at other temperatures (V.V. Iyer, G. Sriram, and J.V. Shanks, unpublished data) and from *Catharanthus roseus* hairy roots (G. Sriram and J.V. Shanks, unpublished data). This was not an artifact of the protein hydrolysis or NMR, since it has neither been reported in isotopomer abundance data from hydrolysates of protein from prokaryotes (e.g. Szyperski, 1995) nor been observed in our data from hydrolysates of 100% ^{13}C-labeled prokaryotic protein. This anomaly was not observed in other Leu atoms. This anomaly suggests that the assumption of Pyr^P as a precursor to Leu δ^1 or the assumed linear metabolic pathway from Pyr^P to Leu δ^1 may be incorrect. However, there exists substantial evidence that Pyr^P is the precursor of Leu δ^1 (Singh, 1999). Also, the observed isotopomer abundances of Val γ^1 and Ile γ^2 agreed with the simulated abundances of Pyr^P. Therefore, it may be likely that the pathway between 2-oxoisovalerate and Leu (the only part of the pathway of branched amino acid synthesis from Pyr^P not shared by Val or Ile) may have other precursors feeding into it and needs further investigation. An alternative explanation of this anomaly is that Leu may be metabolized by pathways not considered in our metabolic model. While this anomaly is still not completely resolved, it points to the fact that such comprehensive flux analysis can draw attention to errors in hypothesized pathways in a metabolic model.

We observed that the hexose nucleotide pools in the cytosol and plastid were not in isotopic equilibrium. This result is supported by the finding that, in *D. carota* cells, the ^{13}C enrichments of the carbon atoms of Suc (synthesized from the cytosolic hexose phosphate pool) and starch (synthesized from the plastidic hexose phosphate pool) were significantly different throughout the period of labeling study (Krook et al., 1998). However, Keeling (1991), Rontein et al. (2002), and Schwender et al. (2003) reported nearly similar enrichments for Suc and starch, which contrasts with our result. Therefore, the equilibration of hexoses between the two compartments may be a function of metabolic demand, and no general conclusion can be made.

On the other hand, our data showed that the T3P pools in the cytosol and plastid have the same isotopomeric composition and were not distinguishable. This has been observed previously by Rontein et al. (2002) and Schwender et al. (2003). One possibility that explains this result is that the two pools may be exchanging rapidly, i.e. they are in equilibrium. Another possibility that could account for this result is the absence of enolase in the plastid. Enolase catalyzes the conversion of 3PG to PEP, and its absence has been reported in chloroplasts as well as nonphotosynthetic plastids of various species (Fischer et al., 1997). If it is absent in the plastid, the PEP (and/or pyruvate) required for plastidic biosynthesis may have to be manufactured in the cytosol. This would necessitate the export of T3P from the plastid to the cytosol (by the T3P/phosphate transporter) and the import of PEP in the opposite direction (by the PEP/phosphate transporter; Streatfield et al., 1999). This model suggests a single, lower glycolytic pathway in many plastids.

Our data showed negligible photosynthetic carbon assimilation, although the cotyledons were green

during culture. This agrees with ^{13}C label data from *B. napus* embryos (Schwender and Ohlrogge, 2002) and also with studies by Chao et al. (1995), who found that developing soybean embryos that retained chlorophyll expressed the photosynthetic mRNAs *Lhcb* and *RbcS* in insignificant amounts during the filling period (period of storage protein accumulation). Also, studies by Eastmond and Rawsthorne (1998) concluded that the accumulation of storage products by embryos was largely heterotrophic with a minor photosynthetic contribution. Furthermore, we observed that a photorespiratory pathway was not necessary to account for the observed differences between the isotopomer abundances of Ser and other amino acids that reflect the T3P pool. Together, these results signify that green embryos are chloroplast-containing tissue functioning heterotrophically and lacking any significant photosynthetic or related function.

We detected a substantial flux through the oxPPPs in the cytosol and plastid. In plants, the function of the oxPPP is believed to be 2-fold: provision of reductant (particularly NADPH) in the plastid and hexose metabolism in the cytosol. In the plastid, the NADPH generated in the oxPPP is used for lipid and protein synthesis, nitrogen or Gln assimilation, and combating oxidative stress (Hauschild and von Schaewen, 2003). Since NADPH does not cross membranes, the plastid requirement of NADPH must be generated within the same compartment. We determined the plastidic NADPH requirement and availability in our system, based on the evaluated fluxes, to be 22.28 ($\pm$0.22) μmol d^{-1} cotyledon^{-1}. This includes the amounts needed for de novo amino acid and fatty acid synthesis, and for Gln assimilation. The availability of NADPH from the plastidic oxPPP is 21.80 ($\pm$9.93) μmol d^{-1} cotyledon^{-1}. Thus, the plastidic oxPPP provides 98% ($\pm$45%) of the NADPH requirement. This points to the oxPPP as a substantial contributor to the NADPH pool in the plastid. This is in concordance with previous studies that have found that the plastidic oxPPP is stimulated in response to high demands for NADPH (Hauschild and von Schaewen, 2003) and is coupled to Glu assimilation (Esposito et al., 2003).

However, our value of NADPH availability from the oxPPP is higher than that calculated by Schwender et al. (2003) for developing *B. napus* embryos. (Schwender et al. estimated the oxPPP to provide 22% to 45% of the plastidic requirement.) This difference could be explained by the fact that *B. napus* embryos predominantly synthesize lipids, whereas soybean embryos synthesize both protein and lipids. The demand for reductant could be met differently in these systems. Further, the high Glu assimilation in our system may have stimulated the oxPPP.

We were able to distinguish between the fluxes through the reversible nonoxidative limbs of the oxPPP in the cytosol and the plastid. These fluxes are catalyzed by transketolase and transaldolase and were observed by us to be substantial in the plastid and small or negligible in the cytosol. Ireland and Dennis (1980) have detected these enzymes in the plastid and cytosol of soybean nodules, indicating that the soybean genome may contain genes encoding plastidic and cytosolic isoforms of these enzymes. However the results reported here indicate that in our system, they are either not expressed or are not sufficiently active in the cytosol. The compartmentation of these enzymes in plants has been subject to investigation recently but still remains an open question. For example, Debnam and Emes (1999) found that in spinach (*Spinacia oleracea*) and pea (*Pisum sativum*), transketolase or transaldolase activity was confined only to the plastid, whereas in tobacco (*Nicotiana tabacum*) these enzymes were found in both compartments. Further, Eicks et al. (2002) found that all putative transketolase and transaldolase genes in Arabidopsis have a plastid-targeting sequence, and they have suggested that exclusive confinement of transketolase and transaldolase to the plastid may be the case in higher plants. However, *Craterostigma plantagineum* contains both plastidic and cytosolic genes for these enzymes (Bernacchia et al., 1995) and is an exception. Nevertheless, the emerging general picture is one where transketolase and transaldolase operate only in the plastid (Kruger and von Schaewen, 2003). Interestingly, our results are consistent with this model. Since the function of transketolase and transaldolase enzymes is to convert the pentose phosphates formed in the oxPPP to hexose and triose phosphates and return them to glycolysis for further catabolism, it is therefore natural to see high fluxes through them in the plastid in our system, where the pentose phosphates formed in the oxPPP (during NADPH generation; see above) may have no major role.

One possible criticism of our result indicating separate transketolase and transaldolase fluxes in the cytosol and plastid is that the cytosolic nucleotide-diphosphate sugars acting as precursors for protein glycosylation may not be equilibrating isotopically with the cytosolic hexose phosphate pool (and therefore are not derived from cytosolic G6P as assumed in our model) but may be directly derived from Suc synthase with little connection to the hexose phosphate pool. However, since large exchange fluxes have been reported between Suc and the hexose phosphate pool (Dieuaide-Noubhani et al., 1995; Rontein et al., 2002), this criticism may not hold. Secondly, the fluxes calculated for cytosolic and plastidic transketolase and transaldolase, using the assumed model, are consistent with the currently emerging model (substantial transketolase and transaldolase fluxes in the plastid and zero or negligible fluxes of these enzymes in the cytosol; see above) of the pentose phosphate pathway in plants (Kruger and von Schaewen, 2003).

We found that a flux from T3P to F6P had to be included in our model to account for the observed isotopomeric composition of starch. The oxPPP alone could not account for observed labeling pattern. A high T3P $\rightarrow$ F6P flux was detected in the plastid, while a negligible flux was detected in cytosol. The F6P $\rightarrow$

T3P conversion catalyzed by phosphofructokinase is irreversible, and the only plastidic enzyme responsible for a flux in the opposite direction is Fru-1,6-bisphosphatase. Interestingly, this enzyme is usually associated with photosynthetic plastids, where it converts the photosynthate to starch for storage. Its existence has been ruled out in heterotrophic tissues, although it has been detected in pea embryos (Entwistle and ap Rees, 1990). Together with this result, our finding suggests an atypical role for plastidic Fru-1,6-bisphosphatase in embryo metabolism.

Plants contain anaplerotic enzymes catalyzing both directions of the PEP/Pyr → OAA/Mal conversion, and the plastidic Mal → Pyr conversion is thought to provide plastidic Pyr and/or NADPH toward biosynthesis. However, we found little cycling between these reactions, and the function of the anaplerotic fluxes appears to be replenishment of the small amount of OAA lost from the TCA cycle to Asp and Asn biosynthesis. We observed a rather small flux from Mal → Pyr in the plastid. This indicates that, in our system, Mal does not substantially contribute carbon toward biosynthesis or NADPH availability.

The GABA shunt has been detected in soybean cotyledons previously (Breitkreuz and Shelp, 1995), and we found that it appears to be preferred over succinate thiokinase reaction of the TCA cycle. We also observed negligible flux through the glyoxylate shunt. This is natural to expect, since the glyoxylate enzymes in embryos are turned on only at the start of germination (Reynolds and Smith, 1995) and during leaf senescence. The glyoxylate shunt metabolizes acetate units resulting from the breakdown of lipids, and in a tissue that primarily accumulates lipids, its activity is anticipated to be insignificant.

CONCLUSION AND FUTURE DIRECTIONS

In this work, we performed ^{13}C-labeling experiments on developing soybean embryos and obtained exhaustive labeling data from sink metabolites by 2-D NMR. It was possible to quantify carbon partitioning through several metabolic processes, including glycolysis, oxPPP, gluconeogenesis, anaplerotic pathways, TCA cycle, and the glyoxylate and GABA shunts. Furthermore, we were also able to distinguish between fluxes in different compartments, based on labeling data of sink metabolites known to be synthesized in separate compartments. To the best of our knowledge, this is the most comprehensive flux analysis of a plant system to date. The experimental methodology employed in this work has the potential to become a high-throughput one. Further reduction of the sample size and duration of labeling period should be possible and could be optimized. The computer program developed to calculate fluxes from the labeling data is generic. We expect these features to increase the applicability of flux analysis in plants.

As demonstrated here, flux analysis can provide insights on physiology and function. Comparison of fluxes between genetic or environmental variants can provide valuable information about the effects of genetic or environmental manipulations on the physiology. This is particularly relevant in the context of the recent upsurge in plant metabolic engineering (Hanson and Shanks, 2002). Together with high-throughput data on transcripts, proteins, and metabolites, systemic flux data can provide the basis for understanding the functioning of plants from a systems biology perspective (Sweetlove et al., 2003). Work is under way in our laboratory to evaluate fluxes in soybean embryos grown in different environments and in another plant system. Using recent theoretical developments on flux identifiability (Isermann and Wiechert, 2003), we are also working toward designing labeling experiments on plant systems with judicious combinations of labeled substrates so as to increase the flux information available from them.

MATERIALS AND METHODS

Soybean Cotyledon Culture

Soybean (*Glycine max* cv Evans) was grown in a growth chamber at 27°C/20°C and 14-h photoperiod. Eighteen days after flowering, pods were harvested from the central section of the main stem and embryos isolated for in vitro culture. Three cotyledons were selected for uniform initial size (100–120 mg fresh weight) and cultured aseptically in 20 mL of liquid medium containing 146 mM Suc (10% [w/w] U-^{13}C, 90% [w/w] commercial, with a natural ^{13}C abundance of 1.1%) and 37 mM Gln (commercial, natural ^{13}C abundance of 1.1%) as the only carbon sources. This labeling technique is termed biosynthetically directed fractional ^{13}C labeling (Szyperski, 1995). U-^{13}C Suc was purchased from Isotec (Miamisburg, OH). The in vitro culture was maintained at 25°C, 100 rpm, and approximately 100 $\mu E\ m^{-2}\ s^{-1}$ light intensity. After 6 d of culture, cotyledons were harvested, rinsed with nonlabeled medium, and lyophilized at −50°C and 133×10^{-3} mbar for 72 h. The lyophilized embryos were finely ground for further processing.

Protein Extraction, Hydrolysis, Amino Acid Quantification, and NMR Sample Preparation

Protein was extracted from ground samples in 100 mM phosphate buffer, pH 7.2, at 4°C for 15 min. The extract was repeated four times, and the consolidated supernatant was assayed for protein using the Bradford test (Bio-Rad Laboratories, Hercules, CA).

Protein hydrolysis was performed in hydrolysis tubes (Pierce Endogen, Rockford, IL), to which 6 N hydrochloric acid was added in the 0.5 mL of HCl:400 μg of protein. The hydrolysis tube was evacuated, flushed with nitrogen to remove residual oxygen, and reevacuated. Hydrolysis was performed at 150°C for 4 h. The acid in the hydrolysate was evaporated in a Rapidvap evaporator (Labconco, Kansas City, MO). The residue was redissolved in 2 mL of deionized water, lyophilized for 72 h, and dissolved in 500 μL of D_2O in an NMR tube. The pH of the NMR sample was adjusted to 0.5 using DCl. Amino acids in the sample were quantified by HPLC, after derivatization with phenylisothiocyanate to produce phenylthiocarbamyl amino acid derivatives, which were eluted by a reverse-phase C_{18} silica column, with detection at 254 nm.

Extracellular Fluxes and Fluxes Contributing to Biomass

Biomass growth was quantified by measuring embryo fresh weight. Protein and proteinogenic amino acid proportions in the biomass were determined as above. Lipids were extracted in hexane at 45°C and quantified by weight. Suc consumption was measured using HPLC. The measurements related to biomass fluxes are listed in Supplemental Material II.

NMR Spectroscopy

Two-dimensional [^{13}C, ^{1}H] HSQC NMR spectra (Bodenhausen and Ruben, 1980) were collected on a Bruker Avance DRX 500 MHz spectrometer (Bruker Instruments, Billerica, MA) at 298 K. The reference to 0 ppm was set using the methyl signal of dimethylsilapentanesulfonate (Sigma, St. Louis) as an internal standard. The resonance frequency of ^{13}C and ^{1}H were 125.7 MHz and 499.9 MHz, respectively. The spectral width was 5,482.26 Hz along the ^{1}H (F2) dimension and 5,028.05 Hz along the ^{13}C (F1) dimension. Peak aliasing was used in order to minimize the sweep width along the F1 dimension. The number of complex data points was 1,024 (^{1}H) $\times$ 900 (^{13}C). A modification of the INEPT (insensitive nuclei enhanced by polarization transfer) pulse sequence was used for acquiring HSQC spectra (Bodenhausen and Ruben, 1980). The number of scans was generally set to 16. Assignment of amino acid peaks on the HSQC spectrum was verified using 2-D [^{1}H, ^{1}H] total correlation (TOCSY) and 3-D [^{13}C, ^{1}H, ^{1}H] TOCSY spectra (Braunschweiler and Ernst, 1983), which were acquired with a 100% labeled protein sample. While acquiring TOCSY spectra, the DIPSI-2 sequence (Shaka et al., 1988) was used for isotropic mixing, with a mixing time of 76 ms.

The software Xwinnmr (Bruker) was used to acquire all spectra, and the software NMRView (Johnson and Blevins, 1994; available at http://onemoonscientific.com/nmrview) was used to quantify nonoverlapping multiplets on the HSQC spectrum. To quantify overlapping multiplets (α-amino acid and LVA peaks), which could not be processed with NMRView, a peak deconvolution software was written. This software was based on a spectral model proposed by van Winden et al. (2001). Additionally, 2-D spectra were obtained that were *J*-scaled along the F1 dimension, by incorporating pulse sequences described by Willker et al. (1997) and Brown (1984) into the HSQC pulse sequence. *J*-scaling increases multiplet separation by an even integral factor *J* and eliminates multiplet overlap. *J*-scaling factors of 6 or 8 were employed.

We verified that the [^{13}C, ^{1}H] experiment employed by us (and the subsequent spectral analysis) can accurately measure isotopomer abundances, by performing it on two samples containing known quantities of three commercial isotopomers of Ala (a representative amino acid). Details are provided in Supplemental Material III.

Flux Evaluation Methodology and Computer Program

Fluxes were evaluated from isotopomer data by using isotopomer balancing and a global routine. The objective of this flux evaluation procedure is to evaluate a set of stoichiometrically feasible fluxes (per the metabolic network supplied by the user) that best accounts for the measured isotopomer abundances and extracellular flux measurements. Furthermore, uniqueness of the evaluated flux solution was ensured and statistical analysis was performed. The computer program that evaluates fluxes, NMR2Flux, is implemented in the programming language C, on the Red Hat Linux operating system. All mathematical and computational details are presented in Supplemental Material IV to VI.

Upon request, all novel materials described in this paper (flux evaluation program NMR2Flux, modified NMR pulse sequences, and peak deconvolution software) will be made available in a timely manner for noncommercial research purposes, subject to the requisite permission from any third-party owners of all or parts of the material. Obtaining any permissions will be the responsibility of the requestor.

ACKNOWLEDGMENTS

We thank Dr. Eve Wurtele (Department of Botany, Iowa State University) for helpful discussions on this work and for her comments on the manuscript, Dr. Amy Andreotti (Department of Biochemistry, Biophysics and Molecular Biology, Iowa State University) for a gift of 100% ^{13}C-labeled protein, Dr. Louisa B. Tabatabai (Department of Biochemistry, Biophysics and Molecular Biology, Iowa State University) for consultations on protein hydrolysis, and Curtis C. Clifton (Department of Computer Science, Iowa State University) for useful information on UML (Universal Modeling Language).

Received July 26, 2004; returned for revision August 6, 2004; accepted August 6, 2004.

LITERATURE CITED

Bacher A, Rieder C, Eichinger D, Arigoni D, Fuchs G, Eisenreich W (1999) Elucidation of novel biosynthetic pathways and metabolite flux patterns by retrobiosynthetic NMR analysis. FEMS Microbiol Rev **22:** 567–598

Baldwin TC, Handford MG, Yuseff MI, Orellana A, Dupree P (2001) Identification and characterization of GONST1: a golgi-localized GDP-mannose transporter in Arabidopsis. Plant Cell **13:** 2283–2295

Bernacchia G, Schwall G, Lottspeich F, Salamini F, Bartels D (1995) The transketolase gene family of the resurrection plant *Craterostigma Plantagineum*: differential expression during rehydration phase. EMBO J **14:** 610–618

Bewley JD, Black M (1994) Seeds: germination, structure and composition. *In* JD Bewley, M Black, eds, Seeds: Physiology of Development and Germination. Plenum Press, New York

Bodenhausen G, Ruben DJ (1980) Natural abundance nitrogen-15 NMR by enhanced heteronuclear spectroscopy. Chem Phys Lett **69:** 185–189

Bourguignon J, Rebeille F, Douce R (1999) Serine and glycine metabolism in higher plants. *In* BK Singh, ed, Plant Amino Acids: Biochemistry and Biotechnology. Marcel Dekker, New York

Braunschweiler L, Ernst RR (1983) Correlation transfer by isotropic mixing: application to proton correlation spectroscopy. J Magn Reson **53:** 521–528

Breitkreuz KE, Shelp B (1995) Subcellular compartmentation of the γ-aminobutyrate shunt in protoplasts from developing soybean cotyledons. Plant Physiol **108:** 99–103

Brown LR (1984) Differential scaling along ω_1 in COSY experiments. J Magn Reson **57:** 513–518

Casati P, Drincovich MF, Edwards GE, Andreo CS (1999) Malate metabolism by NADP-malic enzyme in plant defense. Phytosynth Res **61:** 99–105

Cavanagh J, Fairbrother WJ, Palmer AG, Skelton NJ (1996) Protein NMR Spectroscopy: Principles and Practice. Academic Press, San Diego

Chao WS, Liu V, Thomson WW, Platt K, Walling LL (1995) The impact of chlorophyll-retention mutations d7d2 and cyt-G7: during embryogeny in soybean. Plant Physiol **107:** 253–262

Chollet R, Vidal J, O'Leary MH (1996) Phosphoenolpyruvate carboxylase: a ubiquitous highly regulated enzyme in plants. Annu Rev Plant Physiol Plant Mol Biol **47:** 273–298

Coates SW, Gurney T, Sommers LW, Yeh M, Hirschberg CB (1980) Subcellular localization of sugar nucleotide synthases. J Biol Chem **255:** 9225–9229

Debnam PM, Emes MJ (1999) Subcellular distribution of the enzymes of the oxidative pentose phosphate pathway in root and leaf tissues. J Exp Bot **340:** 1653–1661

Dey PM, Harborne JB (1997) Plant Biochemistry. Academic Press, San Diego

Dieuaide-Noubhani M, Raffard G, Canioni P, Pradet A, Raymond P (1995) Quantification of compartmented metabolic fluxes in maize root tips using isotope distribution from ^{13}C- or ^{14}C-labeled glucose. J Biol Chem **22:** 13147–13159

Doyle JJ, Schuler MA, Godette WD, Zenger V, Beachy RN (1986) The glycosylated seed storage proteins of *Glycine max* and *Phaseolus vulgaris*. J Biol Chem **261:** 9228–9238

Drincovich MF, Casati P, Andreo CS (2001) NADP-malic enzyme from plants: a ubiquitous enzyme involved in different metabolic pathways. FEBS Lett **490:** 1–6

Eastmond PJ, Rawsthorne S (1998) Comparison of the metabolic properties of plastids isolated from developing leaves or embryos of *Brassica napus*. J Exp Bot **49:** 1105–1111

Eicks M, Maurino V, Knappe S, Flügge UI, Fischer K (2002) The plastidic pentose phosphate translocator represents a link between the cytosolic and the plastidic pentose phosphate pathways in plants. Plant Physiol **128:** 512–522

Entwistle G, ap Rees TA (1990) Lack of fructose-1:6-bisphosphatase in a range of higher plants that store starch. Biochem J **271:** 467–472

Esposito S, Massaro G, Vona V, Di Martino Rigano V, Carfagna S (2003) Glutamate synthesis in barley roots: the role of plastidic glucose-6-phosphate dehydrogenase. Planta **216:** 637–647

Faik A, Desveaux D, Maclachlan G (2000) Sugar-nucleotide binding and autoglycosylating polypeptides from nasturtium fruit: biochemical capacities and potential functions. Biochem J **347:** 857–864

Fischer K, Kammerer B, Gutensohn M, Arbinger B, Weber A, Hausler RE, Flügge UI (1997) A new class of plastidic phosphate translocators:

a putative link between primary and secondary metabolism by the phosphoenolpyruvate/phosphate antiporter. Plant Cell **9:** 453–462

Girke T, Ozkan M, Carter D, Raikhel NV (2003) Towards a modeling infrastructure for studying plant cells. Plant Physiol **132:** 410–414

Glawischnig E, Gierl A, Tomas A, Bacher A, Eisenreich W (2001) Retrobiosynthetic nuclear magnetic resonance analysis of amino acid biosynthesis and intermediary metabolism: metabolic flux in developing maize kernels. Plant Physiol **125:** 1178–1186

Glawischnig E, Gierl A, Tomas A, Bacher A, Eisenreich W (2002) Starch biosynthesis and intermediary metabolism in maize kernels: quantitative analysis of metabolite flux by nuclear magnetic resonance. Plant Physiol **130:** 1717–1727

Glawischnig E, Tomas A, Eisenreich W, Spiteller P, Bacher A, Gierl A (2000) Auxin biosynthesis in maize kernels. Plant Physiol **123:** 1109–1119

Hanson AD, Shanks JV (2002) Plant metabolic engineering: entering the S curve. Metab Eng **4:** 1–2

Harris RK (1983) Nuclear Magnetic Resonance Spectroscopy: A Physiochemical View. Pitman Books, London

Hauschild R, von Schaewen A (2003) Differential regulation of glucose-6-phosphate dehydrogenase isoenzyme activities in potato. Plant Physiol **133:** 47–62

Hermann KM, Weaver LM (1999) The shikimate pathway. Annu Rev Plant Physiol Plant Mol Biol **50:** 473–503

Ireland RJ, Dennis DT (1980) Isozymes of the glycolytic and pentose-phosphate pathways in storage tissues of different oilseeds. Planta **149:** 476–479

Ireland RJ, Lea PJ (1999) The enzymes of glutamine glutamate asparagines and aspartate metabolism. *In* BK Singh, ed, Plant Amino Acids: Biochemistry and Biotechnology. Marcel Dekker, New York

Isermann N, Wiechert W (2003) Metabolic isotopomer labeling systems. Part II: structural flux identifiability analysis. Math Biosci **183:** 175–214

Jeanneau M, Vidal J, Gousset-Dupont A, Lebouteiller B, Hodges M, Gerentes D, Perez P (2002) Manipulating PEPC levels in plants. J Exp Bot **53:** 1837–1845

Johnson BA, Blevins RA (1994) NMRView: a computer program for the visualization and analysis of NMR data. J Biomol NMR **4:** 603–614

Katagiri F (2003) Attacking complex problems with the power of systems biology. Plant Physiol **132:** 417–419

KEGG (2004) KEGG. Kyoto Encyclopedia of Genes and Genomes. http://www.genome.ad.jp/kegg (September 17, 2004)

Keeling PL (1991) The pathway and compartmentation of starch synthesis in developing wheat grain. *In* MJ Emes, ed, Compartmentation of Plant Metabolism in Non-Photosynthetic Tissues. Cambridge University Press, Cambridge, UK

Krivdin LB, Kalabin GA (1989) Structural applications of one-bond carbon-carbon coupling constants. Prog Nucl Mag Res Spectroscopy **21:** 293–448

Krook J, Vreugdenhil D, Dijkema C, van der Plas LHW (1998) Sucrose and starch metabolism in carrot (*Daucus carota*) cell suspensions analyzed by ^{13}C labeling: indications for a cytosol and a plastid-localized oxidative pentose phosphate pathway. J Exp Bot **49:** 1917–1924

Kruger NJ, von Schaewen A (2003) The oxidative pentose phosphate pathway: structure and organization. Curr Opin Plant Biol **6:** 236–246

Lam HM, Coschigani KT, Oliviera IC, Melo-Oliviera R, Coruzzi GM (1996) The molecular-genetics of nitrogen assimilation into amino acids in higher plants. Annu Rev Plant Physiol Plant Mol Biol **47:** 569–593

Lea PJ, Leegood RC (1999) Plant Biochemistry and Molecular Biology, Ed 2. John Wiley & Sons, Chichester, UK

Lichtner FT, Spanswick RM (1981) Sucrose uptake by developing soybean cotyledons. Plant Physiol **68:** 693–698

Press WH, Teukolsky SA, Vetterling WT, Flannery BP (1992) Numerical Recipes in C: The Art of Scientific Computing, Ed 2. Cambridge University Press, Cambridge, UK

Raikhel NV, Coruzzi GM (2003) Plant Systems Biology. Plant Physiol **132:** 403

Ratcliffe RG, Shachar-Hill Y (2001) Probing plant metabolism with NMR. Annu Rev Plant Physiol Plant Mol Biol **52:** 499–526

Reynolds SJ, Smith SM (1995) The isocitrate lyase gene of cucumber: isolation characterization and expression in cotyledons following seed germination. Plant Mol Biol **27:** 487–497

Rontein D, Dieuaide-Noubhani M, Dufourc EJ, Raymond P, Rolin D (2002) The metabolic architecture of plant cells: stability of central metabolism and flexibility of anabolic pathways during the growth cycle of tomato cells. J Biol Chem **277:** 43948–43960

Roscher A, Kruger NJ, Ratcliffe RG (2000) Strategies for metabolic flux analysis in plants using isotope labeling. J Biotechnol **77:** 81–102

Saravitz CH, Raper CJ (1995) Responses to sucrose and glutamine by soybean embryos grown in vitro. Physiol Plant **93:** 799–805

Sauer U (2004) High-throughput phenomics: experimental methods for mapping fluxomes. Curr Opin Biotechnol **15:** 58–63

Schmidt K, Nørregaard C, Pedersen B, Meisner A, Duus JØ, Nielsen JØ, Villadsen J (1999) Quantification of intracellular metabolic fluxes from fractional enrichment and ^{13}C-^{13}C coupling constraints on the isotopomer distribution in labeled biomass components. Metab Eng **1:** 166–179

Schwender J, Ohlrogge JB (2002) Probing in vivo metabolism by stable isotope labeling of storage lipids and proteins in developing *Brassica napus* embryos. Plant Physiol **130:** 347–361

Schwender J, Ohlrogge JB, Shachar-Hill Y (2003) A flux model of glycolysis and the oxidative pentosephosphate pathway in developing *Brassica napus* embryos. J Biol Chem **278:** 29442–29453

Shachar-Hill Y (2002) Nuclear magnetic resonance and plant metabolic engineering. Metab Eng **4:** 90–97

Shaka AJ, Lee CJ, Pines A (1988) Iterative schemes for bilinear operators: applications to spin decoupling. J Magn Reson **77:** 274–293

Singh BK (1999) Biosynthesis of valine leucine and isoleucine. *In* BK Singh, ed, Plant Amino Acids: Biochemistry and Biotechnology. Marcel Dekker, New York

Soybase (2004) Soybase. National Center for Genome Resources. http://soybase.ncgr.org (September 17, 2004)

Sriram G, Shanks JV (2001) A mathematical model for carbon bond labeling experiments: analytical solutions and sensitivity analysis for the effect of reaction reversibilities on estimated fluxes. *In* LE Erickson, ed, Proceedings of the 31st Annual Biochemical Engineering Symposium, September 8, 2001, Manhattan, KS, pp 45–54

Sriram G, Shanks JV (2004) Improvements in metabolic flux analysis using carbon labeling experiments: bondomer balancing and Boolean function mapping. Metab Eng **6:** 116–132

Stephanopoulos G (1999) Metabolic fluxes and metabolic engineering. Metab Eng **1:** 1–12

Stephanopoulos G (2002) Metabolic engineering: perspective of a chemical engineer. AIChE J **48:** 920–926

Streatfield SJ, Weber A, Kinsman EA, Haüsler RE, Li J, Post-Beittenmiller D, Kaiser WM, Pyke KA, Flügge UI, Chory J (1999) The phosphoenolpyruvate/phosphate translocator is required for phenolic metabolism palisade cell development and plastid-dependent nuclear gene expression. Plant Cell **11:** 1609–1621

Sweetlove LJ, Last RL, Fernie AD (2003) Predictive metabolic engineering: a goal for systems biology. Plant Physiol **132:** 420–425

Szyperski T (1995) Biosynthetically directed fractional ^{13}C-labeling of proteinogenic amino acids. Eur J Biochem **232:** 433–448

Szyperski T (1998) ^{13}C NMR, MS and metabolic flux balancing in biotechnology research. Q Rev Biophys **31:** 41–106

van Winden W, Schipper D, Verheijen P, Heijnen J (2001) Innovations in generation and analysis of 2D [^{13}C, ^{1}H] COSY NMR spectra for metabolic flux analysis purposes. Metab Eng **3:** 322–343

Wheeler GL, Jones MA, Smirnoff N (1998) The biosynthetic pathway of vitamin C in higher plants. Nature **393:** 365–369

Wiechert W (2001) ^{13}C metabolic flux analysis. Metab Eng **3:** 195–206

Wiechert W, Möllney M, Isermann N, Murzel M, de Graaf AA (1999) Bidirectional reaction steps in metabolic networks: III. Explicit solution and analysis of isotopomer labeling systems. Biotechnol Bioeng **66:** 69–85

Wiechert W, Murzel M (2001) Metabolic isotopomer labeling systems, Part I: global dynamic behavior. Math Biosci **169:** 173–205

Willker W, Flögel U, Leibfritz D (1997) Ultra-high-resolved HSQC spectra of multiple-^{13}C-labeled biofluids. J Magn Reson **125:** 216–219

Wüthrich K (1976) NMR in Biological Research: Peptides and Proteins. North Holland, Amsterdam

Yamauchi F, Yamagishi T (1979) Carbohydrate sequence of a soybean 7S protein. Agric Biol Chem **43:** 505–510